Molybdopterin Radical in Bacterial Aldehyde Dehydrogenases†

Dion M. A. M. Luykx, Johannis A. Duine, and Simon de Vries*

Kluyver Institute of Biotechnology, Section Enzymology, Delft University of Technology, Julianalaan 67, 2628 BC Delft, The Netherlands

Received December 3, 1997; Revised Manuscript Received March 12, 1998

ABSTRACT: The EPR spectra of three different molybdoprotein aldehyde dehydrogenases, one purified from *Comamonas testosteroni* and two purified from *Amycolatopsis methanolica*, showed in their oxidized state a novel type of signal. These three enzymes contain two different [2Fe-2S] centers, one flavin and one molybdopterin cytosine dinucleotide, as cofactors all of which are expected to be EPR silent in the oxidized state. The new EPR signal is isotropic with $g = 2.004$ both at X-band and Q-band frequencies, consists of six partially resolved lines, and shows Curie temperature behavior suggesting that the signal is due to an organic radical with $S = {}^1/_2$. The EPR spectra of *Comamonas testosteroni* aldehyde dehydrogenase obtained after cultivation in media containing $^{15}NH_4Cl$ and/or after substitution of H_2O for D_2O show the presence of both nitrogen and proton hyperfine interactions. Simulations of the spectra of the four possible isotope combinations yield a single set of hyperfine coupling constants. The electron spin shows hyperfine interaction with a single $I = 1$ (0.9 mT) ascribed to a N nucleus, with a single $I = {}^1/_2$ (1.5 mT) ascribed to one nonexchangeable H nucleus, and with two, exchangeable, identical $I = {}^1/_2$ spins (0.6 mT) ascribed to two identical exchangeable protons. Taken together, the observations and simulations rule out amino acid residues or flavin as the origin of the radical. The values of the various hyperfine coupling constants are consistent with the properties expected for a molybdenum(VI)−trihydropterin radical in which the N5 atom is engaged in two hydrogen-bonding interactions with the protein. The majority of the electron (spin) density of the radical is located at and around the N5 atom and at the proton bound to the C6 atom of the pterin ring. The EPR spectrum of the molybdopterin radical broadens above 65 K and is no longer detectable above 168 K, indicating that it is not magnetically isolated. The line broadening is ascribed to cross-relaxation with a nearby, rapidly relaxing, oxidized [2Fe-2S] center involving its magnetic $S = 1$ excited state in this process. The amount of radical was apparently not changed by addition of aldehydes or oxidants, but it disappeared upon reduction by sodium dithionite. Therefore, whether the molybdenum(VI) trihydropterin radical as detected here is a functional intermediate in catalysis remains to be investigated further.

Enzymes containing the molybdenum or tungsten pterin cofactor are found in eubacteria and archaebacteria and in lower and higher eukaryotes, and they function as redox enzymes in many different metabolic pathways. They catalyze oxidative hydroxylation reactions of, for example, aromatic heterocycles, aldehydes, formate, carbonmonoxide, or sulfite (*1*, *2*). They also catalyze the reverse of this reaction, the so-called reductive dehydroxylation of, for example, nitrate or DMSO. Both types of hydroxylation reactions are two-electron redox reactions. In the oxidative hydroxylation the hydroxyl group being incorporated into the product is derived from water and not from oxygen. Similarly, in the reductive dehydroxylation, the (hydro)oxo group transferred ends up in water.

The structure of the purified molybdopterin cofactor has been determined by Rajagopalan and co-workers (*3*, *4*). A variant form of the MPT[1] was first detected in CO dehydrogenase (*5*, *6*) and had been identified as molybdopterin cytosine dinucleotide (MCD) in which the nucleotide is attached to the MPT via a pyrophosphate linkage (cf. Figure 9). Later, more variants in the type of nucleotide have been detected, that is, adenosine, guanosine, or hypoxanthine (see ref *7* for an overview). So far molybdopterins attached to a nucleotide have been found exclusively in prokaryotes. Enzymes containing the MPT without a nucleotide have been found both in prokaryotes and in eukaryotes.

Recently, the knowledge of the structure and function of molybdopterin- or tungstopterin-containing enzymes has greatly increased owing to the determination of the 3D structures of four of these enzymes, the aldehyde ferredoxin oxidoreductase from *Pyrococcus furiosus* (*8*), the aldehyde oxidoreductase from *Desulfovibrio gigas* (*9*), the DMSO reductase from *Rhodobacter sphaeroides* (*10*), and the formate dehydrogenase H from *Escherichia coli* (*11*). Two important new findings with respect to the structure of the pterin moiety have emerged from these studies. First, the enzyme-bound pterin system[2] is a nonplanar three-ringed structure (cf. Figure 9) and not a two-ringed system as

† Part of this work has been financed by a grant from EC (Biotechnology Bridge Program, Contract CT90−0157).

* Corresponding author Tel: ++31-15-278-5139. Fax: ++31-15-278-2355. E-mail: s.devries@stm.tudelft.nl.

[1] Abbreviations: MPT, molybdopterin cofactor; MCD, molybdopterin cytosine dinucleotide; AlDH, aldehyde dehydrogenase from *Comamonas testosteroni*; FEDH, DL-AlDH, aldehyde dehydrogenases from *Amycolatopsis methanolica*.

S0006-2960(97)02972-3 CCC: $15.00
Published on Web 07/21/1998

proposed for the free pterin (*4*, *12*). The redox state of the pterin ring system is formally the same as that of the tetrahydrobiopterin. Pterin model compounds in the tetrahydro redox state are nonplanar (*13*, *14*). The observation in all four crystal structures that the three-ringed pterin is nonplanar is consistent with the tetrahydro redox state of the pterin and not with a dihydro redox state (a possible exception may be the Q-molybdopterin ring in DMSO reductase (*15*)). In all four crystal structures, the pterin ring system is observed to be engaged in many hydrogen bonds with residues from the protein. The second new finding, in three of these enzymes but not in the *D. gigas* enzyme, was the presence of a so-called bis-molybdopterin structure in which the Mo or W atom is coordinated by four sulfur atoms derived from two pterin rings (*8*, *16*).

The aldehyde oxidoreductase from *D. gigas* is a homodimer and catalyzes the oxidation of aldehydes to carboxylic acids (*17*, *18*). This enzyme, which shares many characteristics with xanthine oxidase, contains two different types of [2Fe-2S] clusters but lacks FAD. The molybdenum atom is coordinated to two dithiolene sulfur atoms derived from a single pterin (the MCD) and further to two oxygen ligands and one sulfido group (*9*). Recently, a detailed proposal for its mechanism of action describing the chemistry at the molybdenum center has been put forward on the basis of the crystal structures of various forms of the enzyme (*19*).

We have previously described the purification and characterization of the NAD-independent aldehyde dehydrogenases from *Comamonas testosteroni* (AlDH) (*20*) and from *Amycolatopsis methanolica* (FEDH (*21*) and DL-AlDH (*22*)). These enzymes can be classified as molybdenum hydroxylases. They catalyze dye-linked oxidation of aldehydes to the corresponding carboxylic acids. These three enzymes have different substrate specificities, and their natural electron acceptors are unknown. Each one consists of three different subunits and contains one molybdopterin cytosine dinucleotide and one FAD and two EPR distinguishable [2Fe-2S] clusters (*23*). The three enzymes show sequence similarity (32− 55%) with the aldehyde oxidoreductase from *D. gigas*. The major apparent difference is the absence of FAD in the *D. gigas* enzyme.

Despite the enormous progress made regarding the structure of molybdo (tungsto) proteins, the role(s) of the pterin moiety itself during catalysis remains to be elucidated. So far indications exist that its redox state is important for overall activity (*24*) and/or in electron transfer (*25*). However, whether molybdopterin acts in a manner similar to that of tetrahydrobiopterin, that is, as an electron donor (cf. ref *26*) in reactions catalyzed by, for example, aromatic amino acid hydroxylases (*27*), is not known. Furthermore, why the molybdenum atom is coordinated to dithiolene sulfur atoms and not to potential ligands of the protein (Cys) is unknown. Is this related to function or to the pathway of biosynthesis of the cofactor (*28*−*30*)? For example, Cys might not able to replace the Mo−O bond as present in molybdate by a Mo−S bond. To answer part of these questions we study the properties of bacterial aldehyde dehydrogenases. In this paper we describe the properties of a novel EPR signal present in three aldehyde dehydrogenases "as isolated". Since all known prosthetic groups in these three enzymes should be EPR silent, the "as isolated" enzyme is oxidized, which is the case for other molybdenum hydroxylases except for the presence of some Mo(V), the detection of a novel EPR signal was unexpected. This paper deals with the structural characterization of the species yielding this new EPR signal. We have performed various isotope substitution experiments, EPR spectroscopy at X- and Q-band frequencies, and EPR spectral simulations leading to the proposal that the EPR signal is due to a molybdenum(VI) trihydropterin radical. A possible role of this radical in catalysis, in particular in electron transfer, will be discussed.

EXPERIMENTAL PROCEDURES

Growth of *C. testosteroni* (ATCC 15667) and isolation of the aldehyde dehydrogenase was as described (*20*, *23*). The ^{15}N-containing AlDH was obtained by cultivation of *C. testosteroni* on mineral medium containing, per liter, 1 g of $^{15}NH_4Cl$ and 4 g of K_2SO_4 replacing 3 g of $(NH_4)_2SO_4$. The ^{95}Mo or ^{98}Mo derivatives of AlDH were obtained by growing *C. testosteroni* in 2 μM $(Na)_2{}^{95}MoO_4$ or $(Na)_2{}^{98}MoO_4$, respectively, instead of 0.1 μM $(Na)_2MoO_4$. $(Na)_2{}^{95}MoO_4$ and $(Na)_2{}^{98}MoO_4$ were prepared from ^{95}Mo or ^{98}Mo. ^{95}Mo or ^{98}Mo (each 0.1 mmol) was dissolved in 1 mL of nitric acid. After centrifugation of the sample at 14 000 rpm for 10 min, the supernatant was removed. The disodium molybdate isotopes were obtained by dissolving the remaining pellet in 0.5 mL of 1 M NaOH. Quantitative determination of molybdenum was as in ref *31*. Samples of the *C. testosteroni* aldehyde dehydrogenase in D_2O were obtained by dilution in 20 mM MOPS (pH 7.0) made up in 99.8% D_2O followed by concentration until a final D_2O concentration >99% had been obtained. This procedure lasted about 40 min after which the EPR sample was frozen. To study whether protons were exchanged at a longer time scale, the sample was thawed and incubated in ice for another 7 h. This shape of the EPR signal did not change further (see also text). *A. methanolica* (NCIB 11946) was cultivated as described in ref *21* to obtain FEDH and cultivated as described in ref *22* to obtain DL-AlDH.

UV/vis spectra were measured in cells of 1 cm path length at room temperature with a Hewlett-Packard HP 8452 A diode array spectrophotometer. EPR spectra at X-band frequencies were recorded with a Varian E-9 spectrometer. The magnetic field and microwave frequency were determined with a AEG Kernresonanz-Magnetfeldmesser and a HP 5245L electronic counter, respectively. This spectrometer has been equipped with a home-built He flow system. Q-band EPR spectra were recorded as described in ref *32*.

EPR spectra were simulated with a program specifically written for the MacIntosh PowerPC (68k processor) using CodeWarrior 5, Metroworks Pascal 1.0 software. The expression for the line width used to simulate the anisotropic

[2] The nomenclature of molybdopterins is ambiguous with respect to the redox state of the pterin moiety which may lead to confusion concerning some of the conclusions drawn in this paper. Recent findings (referred to in the text and in the legend to Figure 9) have shown that the pterin ring system is a three-ringed and not a two-ringed system. As a consequence, the redox state of the molybdopterin *in situ* is the same as that of tetrahydrobiopterin, for example. The molybdopterin radical that we describe below is one electron more oxidized than the tetrahydro-redox state and is therefore called a Mo(VI)−trihydropterin radical. Furthermore, we use the old numbering of the atoms of the pterin ring. Since the pterin ring system is a three-ringed system, numbering should actually start at the pyran oxygen atom.

Table 1: Hyperfine Coupling Constants Used To Simulate the Four Spectra of the Mo(VI) Trihydropterin Radical Shown in Figure 4

	$I = 1^a$				$I = 0.5^a$		
nucleus	^{14}N	^{2}D	^{2}D	^{1}H	^{1}H	^{1}H	^{15}N
^{14}N, H_2O	0.9[b]			1.5	0.6	0.6	
^{14}N, D_2O	0.9	0.1	0.1	1.5			
^{15}N, H_2O				1.5	0.7	0.7	1.2
^{15}N, D_2O		0.1	0.1	1.5			1.2

[a] Nuclear spin. [b] Values for the various hyperfine coupling constants expressed in milliteslas are accurate to about ±0.08 mT. Larger deviations from the values listed lead to unacceptable discrepancies (e.g., in the number of (partially) resolved lines) between experimental and simulated spectra. Range of the line width parameters (dependent on the simulation, see Materials and Methods): 0.6 mT < W_r <0.9 mT; −0.1 < B < −0.3; 0.5 < C < 1.0. An isotropic value of g = 2.004 was used in all simulations.

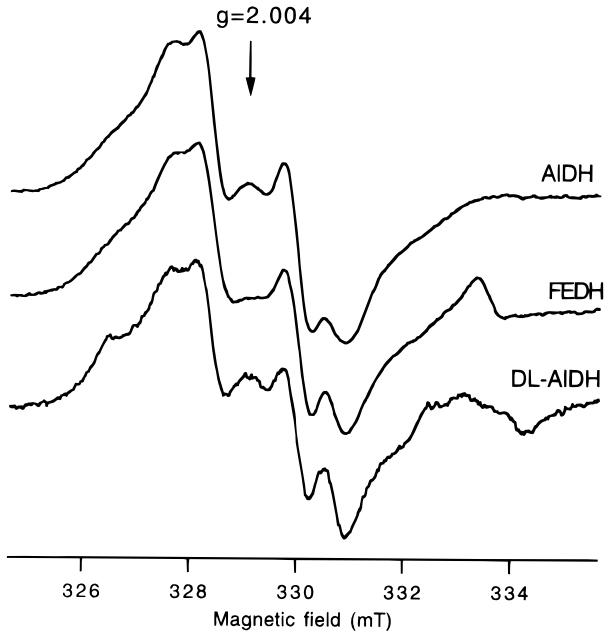

FIGURE 1: X-band EPR spectra of the three different bacterial aldehyde dehydrogenases as isolated. EPR conditions: frequency, 9.236 GHz; modulation amplitude, 0.2 mT; microwave power, 80 μW; temperature, 38 K. NB only the g = 2 region is shown. No other EPR signals were present in the enzymes as isolated except for a small signal at g = 4.3 due to adventitious iron. The signal around 333 mT in, for example, the middle trace is due to some Mo(V) present. See text for further details.

line width of the EPR signal was

$$W = W_r(1 + BM_I + C(M_I)^2)$$

In this expression M_I refers to the "central nucleus" which in the simulations shown is either the ^{14}N or the ^{15}N nucleus (cf. refs *33*, *34*). Since the one nucleus has I = 1 and the other I = 0.5, the values of the line width parameters (W_r, B, and C) used in the various simulations are somewhat different (see legends to Figure 4 and Table 1).

RESULTS

Figure 1 shows the X-band EPR spectra in the g = 2 region of the three different bacterial aldehyde dehydrogenases as isolated. As we have shown previously (*20*, *23*), these enzymes contain the same complement of prosthetic groups as, for example, xanthine oxidase, namely FAD, two different [2Fe-2S] clusters, and a Mo pterin cofactor, the

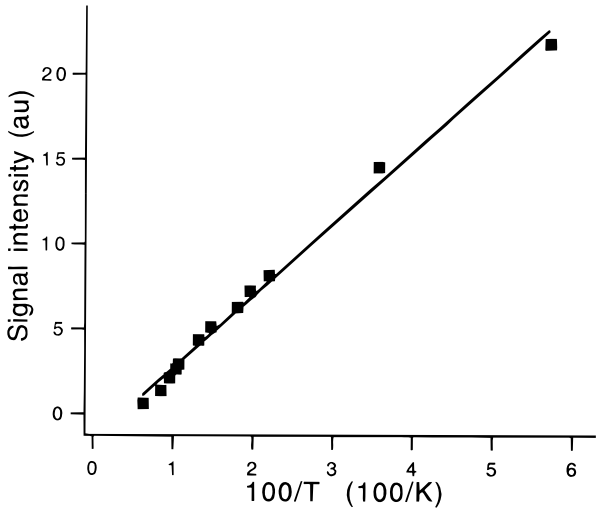

FIGURE 2: Curie plot for the g = 2.004 EPR signal from aldehyde dehydrogenase from *C. testosteroni*. The signal intensity was determined by double integration of the EPR spectrum of the g = 2.004 signal at various temperatures. To compare the values of the double integral, appropriate corrections were made for differences in experimental conditions such as differences in gain, modulation amplitude, and microwave power. Determinations below 15 K are not included because the signal was already saturated at the lowest microwave power (~1 μW at X-band) experimentally accessible precluding an accurate calculation of the signal intensity. NB: Essentially similar relations between temperature and signal intensity were found for the two aldehyde dehydrogenases from *A. methanolica* (data not included).

cytosine−dinucleotide derivatized molybdopterin. Control samples monitored optically and by EPR in which ferricyanide and/or Wurster's Blue were added as oxidants indicate that FAD and the two [2Fe-2S] clusters in all three enzymes were completely oxidized; addition of these oxidants did not change the intensity of the g = 2 signal (data not shown). Neither FAD nor [2Fe-2S] clusters show EPR signals when oxidized; hence the presence of an EPR signal in these three aldehyde dehydrogenases was unexpected. The major EPR signal which has a peculiar line shape is centered at g = 2.004, which suggests that it is due to an organic radical. Minor, derivative-like signals ($g_{x,y}$ resonance) around 333 mT are observed which originate from Mo(V), the intensity of which is dependent on the type (and somewhat on the batch) of enzyme. The corresponding g_z resonance of this Mo(V) species is at approximately 328 mT. The maximal amount of Mo(V) in the enzymes as isolated (middle trace) corresponds to less than 0.5% of the enzyme concentration.

The EPR signal intensity as a function of temperature, graphically represented in the Curie plot of Figure 2, shows that the g = 2.004 signal behaves like a $S = {}^1/_2$ system between temperatures of 5 and 100 K. Above about 100 K the signal intensity apparently decreases somewhat, an effect in part caused by the increase in line width and change in line shape (*vide infra*). At temperatures above 168 K the signal has broadened beyond detection.

Figure 3 shows a comparison between the X-band and the Q-band spectrum of the g = 2.004 signal. The observation that the Q-band spectrum is very similar to the X-band spectrum further supports the proposal that the EPR signal originates from a $S = {}^1/_2$ system for the following reasons. The finding that the overall "width" of the spectrum, at least when plotted on a magnetic field scale (cf. Figure 3), is

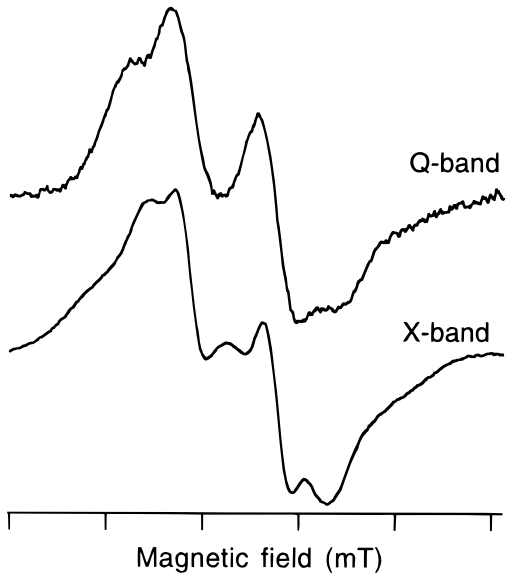

FIGURE 3: X-band and Q-band EPR spectra of the aldehyde dehydrogenase from *C. testosteroni* as isolated. EPR conditions for X-band as in Figure 1. For Q-band: frequency, 35.120 GHz; modulation amplitude, 0.5 mT; microwave power, 20 nW; temperature, 1.6 K. Note that the X-band and Q-band spectra are plotted on the **same** scan width of the magnetic field (10 mT).

independent of frequency leads to the conclusion that the various lines observed are due to (e.g., proton and nitrogen) hyperfine interactions, the strength of which is frequency-independent. Although a spectrum, in terms of overall shape, like the spectrum shown in Figure 3, might be due to $S = 1$ system with fairly small zero-field splitting parameters (D and E), the observation that at Q-band frequency the shape of the spectrum—in particular the spacing between the lines—is basically the same as that at X-band frequency argues against a $S = 1$ system. The major difference between the X-band and Q-band spectra is the peak-to-peak width of the resolved lines. The finding that the various lines in the Q-band spectrum are somewhat broader compared to the X-band spectrum is simply explained by the fact that the relative contribution of g strain to the overall line width is greater at Q-band frequency (*35*).

Determination of the concentration of the $g = 2.004$ signal, assuming it is a $S = {}^1/_2$ system, yields 12% of the enzyme concentration for the enzyme from *C. testosteroni* and 15% and 2% for FEDH and DL-AlDH, respectively, from *A. methanolica*.

Flavin or some amino acid side chains may yield EPR signals at or around $g = 2$. The EPR spectra shown in Figures 1 and 3 are widely different from the EPR spectra of FAD radicals (either the protonated blue or the red anionic radical) in terms of the total width of the spectrum, the peak-to-peak width, or the number of resolved lines (*36*−*38*). The X-band spectrum is, in terms of overall appearance and line shape, most similar to that of the tyrosine radical in, for example, ribonucleotide reductase or Photosystem II (*39*, *40*). However, the X-band and Q-band EPR spectra of tyrosine radicals are very different owing to g anisotropy which is partly resolved at the Q-band. The species in the aldehyde dehydrogenases responsible for the $g = 2.004$ signal shows so little g anisotropy that it is not resolvable at 35 GHz.

To investigate the properties and identity of the radical further, various isotope substitution experiments have been performed. Exchanging water for D_2O leads to a simplification of the EPR spectrum, yielding a spectrum with four well-resolved lines (Figure 4A, lower trace), indicating the presence of exchangeable protons. Prolonged incubation up to 7 h did not change the shape of the spectrum further.

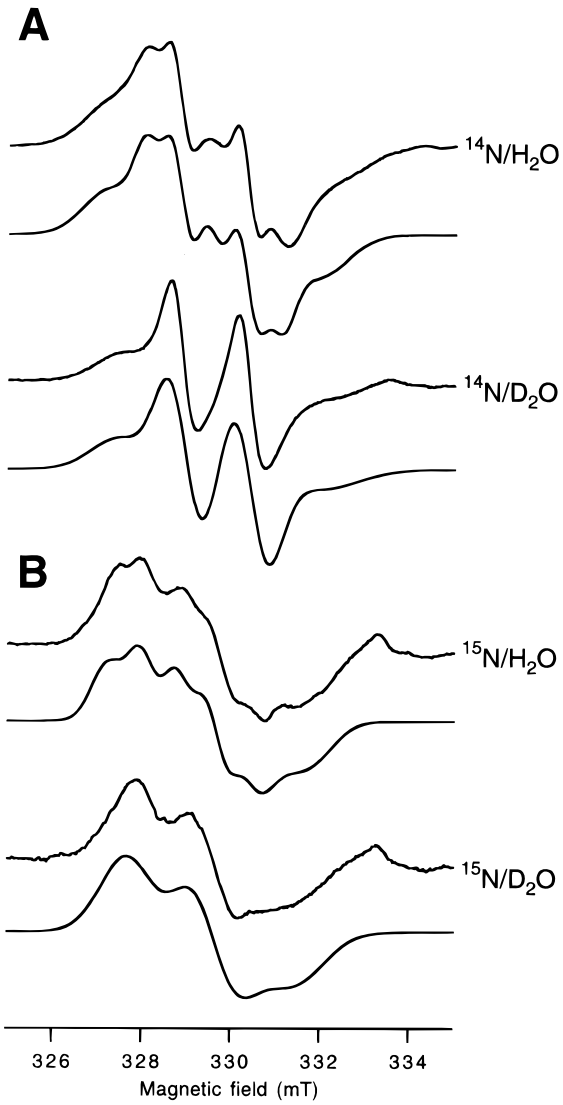

FIGURE 4: X-band EPR spectra of the aldehyde dehydrogenase from *C. testosteroni* grown at ^{14}N (A) or ^{15}N (B) ammoniumchloride and the effect of H_2O/D_2O exchange. The lower trace of each pair of spectra is a computer simulation (see Tables 1 and 2). EPR conditions for all experimental spectra as in Figure 1.

The EPR spectrum of the aldehyde dehydrogenase purified from *C. testosteroni* cultured in the presence of ^{15}N ammoniumchloride is distinctly different from the ^{14}N spectrum (Figure 4B, upper trace). This indicates that the electron spin interacts with one or more nitrogen nuclei. As a consequence, this observation effectively rules out all amino acid based radicals without a N nucleus, in particular tyrosine, as possible candidates yielding the EPR signal. Exchanging water for D_2O in this ^{15}N sample again led to simplification of the EPR signal, in this case consisting of three discernible lines (Figure 4B, lower trace).

The final isotope substitution experiment we performed involved molybdenum. Natural molybdenum consists of a mixture of $^{95,97}Mo$ with ($I = {}^5/_2$) and $^{96,98}Mo$ ($I = 0$). To study possible magnetic interactions between the electron

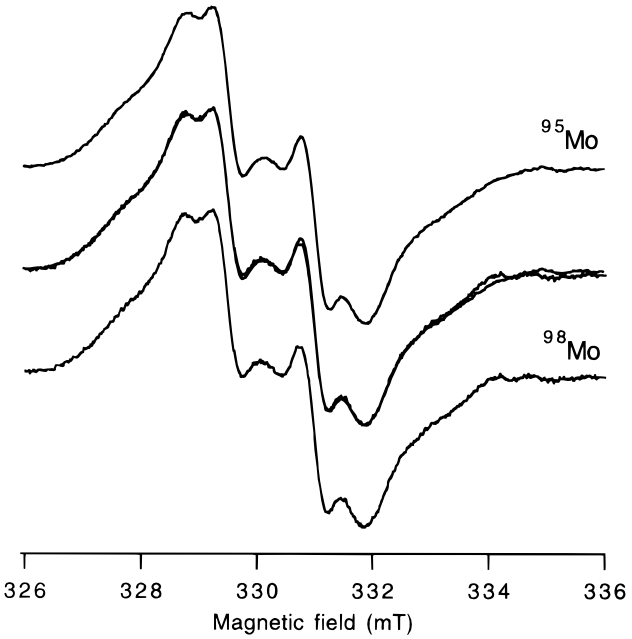

FIGURE 5: X-band EPR spectra of the aldehyde dehydrogenase from *C. testosteroni* grown on ^{95}Mo (upper trace) and ^{98}Mo (lower trace). The middle trace is an overlay of the upper and lower traces. EPR conditions as in Figure 1.

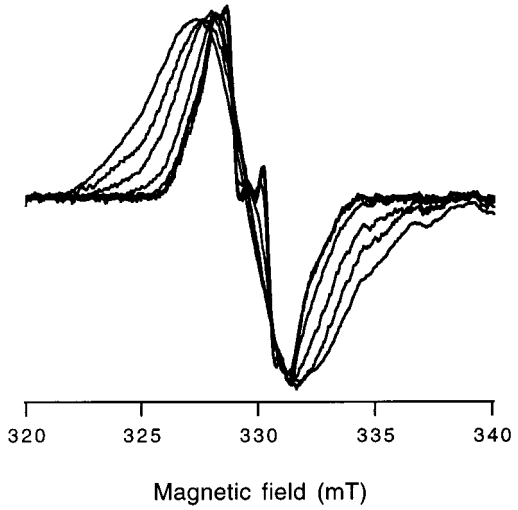

FIGURE 6: X-band EPR spectra of the aldehyde dehydrogenase from *C. testosteroni* recorded at different temperatures showing the increase in line width. The spectra shown have been normalized to the same amplitude. Spectra were recorded at 17, 45, 56, 76, 93, 97, and 118 K.

spin of the $g = 2.004$ signal and the (MoVI) nucleus (not Mo(V)!), *C. testosteroni* was cultivated on the pure isotopes ^{95}Mo and ^{98}Mo and the aldehyde dehydrogenase was purified subsequently. EPR spectra of the two types of preparations are shown in Figure 5. In case of a sufficiently strong magnetic interaction, the ^{95}Mo-containing enzyme should display a (somewhat) broader $g = 2.004$ EPR signal. The overlay of the EPR spectra of the ^{95}Mo- and ^{98}Mo-containing enzymes does not show a significant discernible difference in overall line width; the small differences that are, however, observed can be attributed to small differences in Mo(V) content between the two preparations.

Figure 6 shows that the line shape and overall line width of the radical signal are dependent on temperature. Between 4.2 and 50 K the line shape is fairly constant but above 50 K the signal starts to broaden. The resolution decreases and the signal coalesces into a single featureless signal (Figure 6). A plot of the line width of the radical versus the temperature shows a break at about 65 K (Figure 7A). Above 168 K the signal has broadened beyond detection.

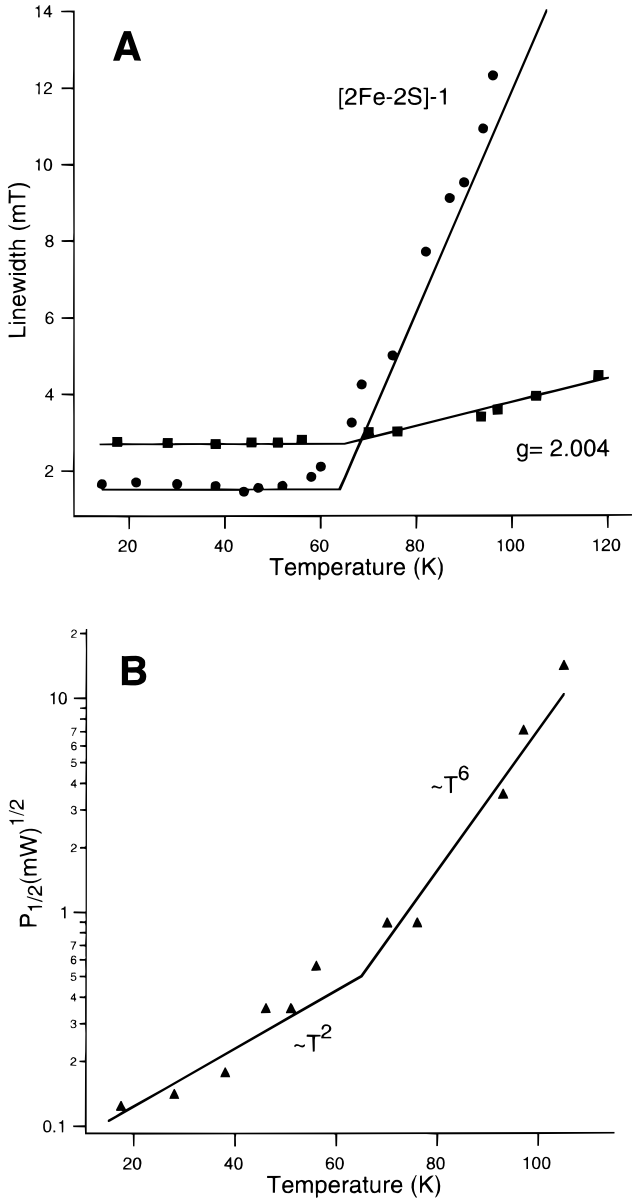

FIGURE 7: (A) Temperature dependence of the line width of the $g = 2.004$ signal (filled squares) and the g_z line of [2Fe-2S]-1 (filled circles); (B) temperature dependence of the power saturation behavior of the $g = 2.004$ signal. (A) The line width is the width (mT) between the point of maximum amplitude of the g_z line of [2Fe-2S]-1 and its half-maximal amplitude, measured at the low-field side of the spectrum (cf. Figure 8). The line width of the $g = 2.004$ signal is the difference (mT) between the points of the maximum and the minimum amplitudes of the signal. (B) $(P_{1/2})^{1/2}$, the square root of the microwave power ($(mW)^{1/2}$) needed for half-saturation, is proportional to the rate of relaxation (cf. ref *39*). The microwave power needed for half-saturation of the EPR signal was determined from power plots (cf. ref *41*) at different temperatures. NB: Determinations of the line width of the $g = 2.004$ signal between 15 and 4.2 K, yielding the same line width as at, for example, 17 K, are not included in A because the EPR signal was already saturated at the lowest microwave power experimentally accessible ($\sim$1 μW at X-band). The break in the curves in A and B occurs in all cases at 65 K. Lines with slopes proportional to T^2 and T^6 are also shown in B.

With increasing temperatures, both the line width and the relative rate of relaxation of the $g = 2.004$ signal, which is proportional to the square root of the microwave power needed for half-saturation, $(P_{1/2})^{1/2}$ (*41*), increase (Figure 7B). The plot of the relative rate of relaxation versus temperature, significantly, shows a break around 65 K, just like the plot of the line width of the $g = 2.004$ signal versus the temperature. Below 65 K the slope is proportional to T^2, consistent with the behavior of an isolated radical; above 65 K the slope is proportional to T^6, suggesting magnetic interaction with a rapidly relaxing paramagnet (*39*).

Figure 8 shows EPR spectra of dithionite reduced aldehyde dehydrogenase from *C. testosteroni*. EPR signals of two different iron−sulfur centers are seen, labeled [2Fe-2S]-1 ($g_{x,y,z} = 1.904, 1.941, 2.023$) and [2Fe-2S]-2 ($g_{x,y,z} = 1.89-1.90, 1.98, 2.092$) (*20, 23*). As we have shown before, these iron−sulfur centers have different relaxation properties. The upper panel indicates the loss of signal intensity of [2Fe-2S]-2 in the temperature range between 14 and 52 K, most conspicious in the decrease of the intensity of the g_z line at $g = 2.09$ and the g_y line at $g = 1.98$. Above 52 K the lines of [2Fe-2S]-2 are too broad to be detected. The line broadening of [2Fe-2S]-2 is due to the increase in the rate of relaxation with temperature. Similarly, the lines of [2Fe-2S]-1 start to broaden due to the increased relaxation rate at temperatures above 55 K (Figure 8, lower panel); at 90 K individual g values are no longer resolved and above 100 K the resonances are too broad to be detected. The plot of the increase in line width of the g_z line of [2Fe-2S]-1 versus temperature (Figure 7A) shows a clear break around 65 K.

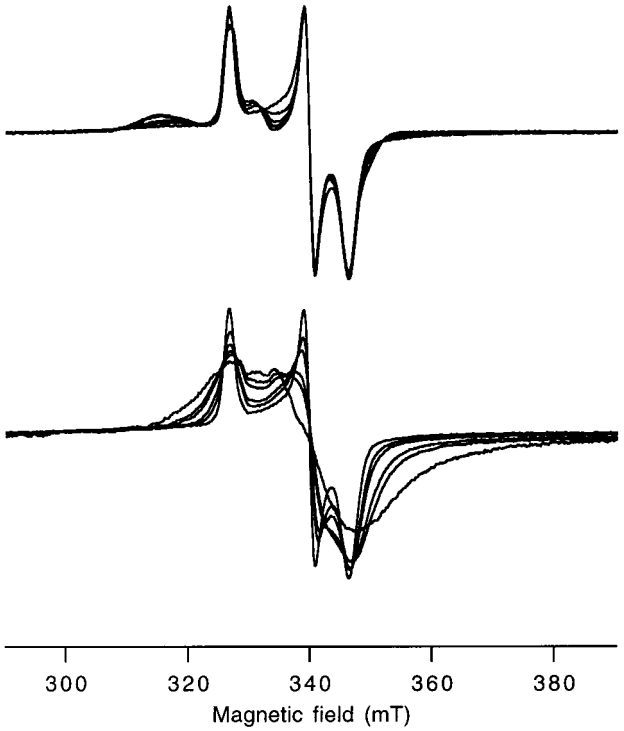

FIGURE 8: EPR signals of the two different [2Fe-2S] clusters in reduced aldehyde dehydrogenase from *C. testosteroni* measured at different temperatures. The upper panel shows the temperature range in which [2Fe-2S]-2 starts to broaden (14, 30, 38, 44, and 52 K), and the lower panel shows the temperature range for which broadening of [2Fe-2S]-1 occurs (52, 58, 60, 67, 75, and 82 K).

DISCUSSION

Elucidation of the Structure of the Species Yielding the g = 2.004 EPR Signal. We have observed a new $g = 2.004$ EPR signal in three different bacterial aldehyde dehydrogenases. The EPR signal is concluded to be due to a $S = {}^1/_2$ spin system since the signal intensity closely follows Curie's law (Figure 2). The observation that at two different frequencies, X-band and Q-band, the EPR signal is very similar in terms of its g value, overall line shape, and overall line width (measured in magnetic field units) is consistent with this proposal. Furthermore the fact that the number and spacing of the various resolved lines is the same in the X-band and Q-band spectra (Figure 3) supports the view that the signal is due to a $S = {}^1/_2$ system interacting with other nuclei. The nature of these interacting nuclei has been investigated by cultivation of *C. testosteroni* in a medium containing $^{15}NH_4Cl$ as a nitrogen source and also by H_2O/D_2O exchange experiments with the purified enzyme. The results obtained in Figure 4 unequivocally show that the electron spin interacts with one or more nitrogen and hydrogen nuclei. Combined, the experimental observations listed above rule out FAD, iron−sulfur centers, and amino acid residues as the origin of the radical. The only other cofactor associated with these three aldehyde dehydrogenases is the cytosin dinucleotide derivative of the molybdopterin, the structure of which is shown in Figure 9. We'll argue in the following that the $g = 2.004$ EPR signal is due to a molybdenum(VI) trihydropterin radical.

Figure 4 shows simulations of the EPR spectra of the radical as present in aldehyde dehydrogenase prepared under 4 different conditions. Although the g anisotropy of the signal is very small (cf. the X-band and Q-band spectra), the line width anisotropy is extremely large. This is clearly seen in the $^{14}N/D_2O$ spectrum in Figure 4 by comparing the difference in line width between the two outer and the two inner lines. Such a large line width anisotropy is, however, present in all 4 spectra of Figure 4 and gives rise to large values of the line width parameters B and C used in the simulations (see Table 1, cf. ref *42*). Owing to the large line width anisotropy, simulation of the signal was not a simple and straightforward matter, even though the signal has an isotropic g value. Preparation of the aldehyde dehydrogenase with 4 different isotopic substitutions proved to be vital to understand how, for example, the number of lines and other details of the spectrum come about. The presence of three lines in the $D_2O/^{15}N$ spectrum and of four lines in the $D_2O/^{14}N$ spectrum is indicative of a strong coupling (1.5 mT) of the electron spin with a $I = {}^1/_2$ nucleus in both spectra plus an additional strong coupling (1.2 or 0.9 mT) with a $I = {}^1/_2$ or 1 nucleus, respectively, in the $D_2O/^{15}N$ spectrum or the $D_2O/^{14}N$ spectrum. As can be seen in Table 1, in all simulations the strong coupling of 1.5 mT ($I = {}^1/_2$) had to be included. The difference between the spectra in H_2O and D_2O is caused by the presence of exhangeable protons interacting with the paramagnetic center. Only when *two* (almost) identical $I = {}^1/_2$ nuclei were included could a satisfactory simulation of the spectra recorded in H_2O be obtained. This concerned, in particular, reproduction of the near absence of intensity (at least in the derivative spectrum) in the central part of the $H_2O/^{14}N$ spectrum. The values for the hyperfine coupling constants of the two nuclei are 0.6 mT ($H_2O/^{14}N$ spectrum) and 0.7 mT ($H_2O/^{15}N$ spectrum) and

should be considered the same given the limits of accuracy of the simulation procedure (see Table 1).

The values for the various hyperfine coupling constants given in Table 1 are apparently different for the different isotope substitutions, but they form in fact a **single** set; that is, the ratio of the values of the hyperfine coupling parameters for ^{14}N- and ^{15}N-containing samples obtained by simulation is, given the limits of accuracy of the simulation and the "goodness of fit", close to the theoretical ratio of 1.40, and a similar reasoning applies to the ^{2}D/^{1}H ratio (0.15). We therefore conclude that the electron spin of the paramagnetic center (in the H_2O/^{14}N sample) interacts with a single strong nitrogen nucleus ($I = 1$, 0.9 mT), with a single strong nonexchangeable proton ($I = {}^1/_2$, 1.5 mT) and with two magnetically indistinguishable H_2O/D_2O exchangeable protons (both $I = {}^1/_2$, 0.6−0.7 mT).

Although observations on molybdopterin radicals in free solution or associated with enzymes have not been reported to our knowledge, literature is available on the structure and properties of tetrahydrobiopterins or more generally on pterin model systems and pterin derivatives including EPR spectroscopic data on monohydro(bio)pterin and trihydro(bio)pterin radicals (*43*−*49*). The EPR spectra of trihydro(bio)pterin radicals in solution are dominated by the strong coupling with the N5 nucleus, by the strong coupling with the exchangeable proton associated with this nucleus H(N5), and by the coupling with the nonexchangeable H(C6) (see Figure 9). In general, the coupling with N8, H(N8), or H(C7) is 3−4-fold lower than with N5, H(N5), or H(C6), respectively (see legend to Table 2). Usually, the values for the hyperfine coupling of N5 and H(N5) are similar in strength (the same holds for N8 and H(N8) in case they are resolved (*48*)). Spin density associated with the pyrimidine ring N and H atoms is too small to be resolved, just as in lumazin- or flavin-free radicals (cf. refs *46*, *47*). Thus in trihydro(bio)pterin free radicals most of the unpaired spin density is located at and around the N5 and C6 nuclei. In contrast, in monohydro(bio)pterin radicals, the unpaired electron (spin) density is much more delocalized in the pyrazin ring, as for example, reflected in the less than 2-fold difference in hyperfine coupling constants for N5, H(N5) compared to N8, H(N8), respectively (*44*).

In general, EPR spectra of radicals associated with proteins show somewhat greater hyperfine coupling constants for C_α or N_α protons (1.5×) compared to the radicals in solution because of the contribution of the anisotropic part of the hyperfine tensors (*37*). This latter interaction is averaged out in the EPR spectra of free radicals recorded in solution due to their rapid tumbling. Given the EPR properties of free pterin radicals listed above, it is most reasonable to assign the $I = 1$, 0.9 mT hyperfine constant to coupling with N5 of the pterin ring and the $I = {}^1/_2$, 1.5 mT to coupling with the nonexchangeable H(C6). To conform to the EPR characteristics of pterin radicals a single exchangeable proton with a coupling of 0.8−1.2 mT is expected. Instead, two identical, exchangeable protons each with a relatively small coupling (0.6−0.7 mT) are required for a satisfactory simulation. To see whether these protons could be H(N5) and H(N8), the EPR spectra were simulated including these two protons, two $I = 1$ nuclei (representing N5 and N8), and the nonexchangeable H(C6). The trial simulations indicated that an additional $I = 1$ nucleus (N8) in the simulation with a coupling greater than about 0.1 mT did not produce satisfactory results (not shown). Consequently, coupling with H(N8) cannot be greater than 0.1 mT, a value significantly different from 0.6 to 0.7 mT. From this we conclude that the two exchangeable protons cannot be assigned to H(N5) and H(N8). We therefore propose that the two exchangeable protons are both bound to N5 (Figure 9). Binding to the same atom, which implies a similar chemical environment, explains not only their similar hyperfine constants but also their relatively small value. The total coupling amounts to approximately 2 × 0.6−0.7 mT

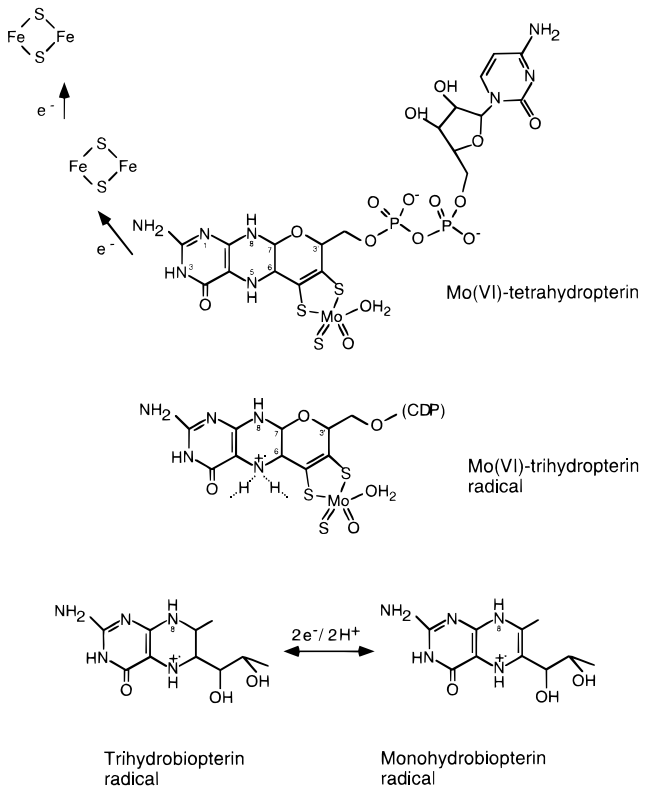

FIGURE 9: Proposal for the structure of the molybdenum(VI) trihydropterin radical. Upper, structure of the molybdopterin (Mo(VI)) cytosin dinucleotide (CDP) as present in aldehyde oxidoreductase from *D. gigas* (*9*). The two [2Fe-2S] clusters are also drawn. In the three aldehyde dehydrogenases from *C. testosteroni* and *A. methanolica* the same molybdopterin derivative is present (*23*). Middle, structure of the molybdenum(VI) trihydropterin radical. Dotted lines from the N5 atom indicate the two hydrogen bonds to the protein. The identity of potential H-donating and H-accepting amino acid residues participating in hydrogen bonding at N5 is unknown. The Mo(VI) trihydropterin radical is one electron more oxidized than the Mo(VI) tetrahydropterin shown in the upper part of the figure. Lower, structure of trihydro and monohydro biopterin radicals. NB: The redox state of the molybdopterin cofactor, which is a nonplanar tricyclic pyranopterin, is the same as that of a tetrahydropterin.

Table 2: Assignment of the Hyperfine Coupling Constants to the Nuclei of the Mo(VI) Trihydropterin Radical (See Also Figure 9)[a]

	nonexchangeable		exchangeable	
nucleus	N	H	H	H
A (mT)	0.9	1.5	0.6	0.6
assignment	N5	H(C6)	H(N5)	H(N5)

[a] Values for trihydrobiopterin free radical (*49*): N5, 0.7 mT; N8, 0.2 mT; H(N5), 0.8 mT; H(N8), 0.2 mT; H(C6), 0.9 mT; H(C7), 0.2 mT.

= 1.2−1.4 mT, a value expected for a single H(N5) in proteins on the basis of the value observed in free pterins. In conclusion, we propose that the radical is a molybdenum(VI)−trihydropterin radical in which the N5 atom is engaged in two hydrogen-bonding interactions with the protein. The majority of the electron (spin) density of the radical is located at and around the N5 atom and at the proton bound to the C6 atom of the pterin ring.

The magnetic and structural properties found for H(N5) in the molybdenum(VI) trihydropterin radical may be compared to those of the flavodoxin semiquinone. This latter flavosemiquinone is a blue semiquinone, that is, protonated at the N5 position (*50*, *51*). The crystal structure shows a single hydrogen bond (2.9 Å) between N5 and the main-chain carbonyl oxygen atom of Gly57 (*52*, *53*). A comparison of the EPR spectra in H_2O and D_2O of the flavodoxin suggests a hyperfine coupling for the single proton at N5 of about 1.1−1.5 mT as compared to 0.8 mT for free flavin radicals (*37*). The crystal structures of the four Mo or W pterin containing enzymes show that the pterin-ring system participates in numerous hydrogen-bonding interactions with amino acid side chains. Regarding protonation/hydrogen bonding at the N5 position, the crystal structures indicate that N5 may participate in two hydrogen-bonding interactions (P-pterin in DMSO reductase (*10*) and both pterins in formate dehydrogenase (*11*)), in one (Q-pterin in DMSO reductase (*10*)), or, apparently, in none (*9*). Residues observed to be involved in hydrogen bonding are Glu, Arg, His, Ser, and water. Although EPR spectroscopy cannot determine the identity of the respective H-donating and H-accepting amino acid residues participating in hydrogen bonding at N5, it predicts that in the aldehyde dehydrogenases from *C. testosteroni* or *A. methanolica* the N5 atom is engaged in two hydrogen bonds. Further confirmation of this and the residues involved has to await elucidation of their 3D structure.

To obtain additional information on the nature of the radical, Mo substitution experiments have been performed. Mo(V) is known to affect the EPR spectrum of the [2Fe-2S]-1 via dipolar coupling, yielding splittings of about 1.0 mT in the resonances of this center (*22*, *54*−*56*). In our preparations, the molybdenum is, however, in the Mo(VI) state and thus far less paramagnetic than Mo(V). Since the Bohr magneton of ^{95}Mo(VI) ($I = {}^5/_2$) is about three times smaller than that of a proton, the hyperfine coupling constant of Mo is about three times smaller. EPR spectral simulations indicate that including a hyperfine coupling constant of 0.1 mT ($I = {}^5/_2$) or greater in addition to the constants listed in Table 2 would yield a measurable increase in the overall width of the spectrum; couplings of 0.03 mT ($I = {}^5/_2$) would measurably change the line shape of the central part of, for example, the $^{14}N/H_2O$ spectrum of the radical. Within experimental resolution, the EPR spectra of ^{95}Mo and ^{98}Mo are the same. This implies a very low electron (spin) density in the pyran ring, not unexpected since it is not conjugated to the pterin ring system. Apparently, the molybdopterin cofactor behaves as a *dinuclear* redox center in which electron (spin) density can be located at the molybdenum atom and/or close to the N5 of the pterin.

Magnetic Coupling between the Molybdenum(VI) Trihydropterin Radical and Oxidized [2Fe-2S]-1. The spectra in Figure 6 show that the EPR signal of the molybdopterin radical starts to broaden at temperatures above 55 K. Above 168 K the signal is undetectable. These phenomena are not expected for a magnetically isolated $S = {}^1/_2$ radical which in general relaxes so slowly that it is detectable by EPR spectroscopy even at room temperature. Figure 7A shows that the temperature dependence of the line broadening of the radical and its rate of relaxation (Figure 7B) both show a break around 65 K. Figure 7A shows that the plot of the line broadening of the EPR spectrum of *reduced* [2Fe-2S]-1 versus temperature also shows a break around 65 K. Line broadening in this latter case is due to an increase in the rate of spin−lattice relaxation ($1/T_1$), that is, the rate at which the absorbed microwave radiation is being transferred to the "bath". The line broadening of the molybdopterin radical and its apparent T^6 dependency (Figure 7B) above 65 K may be explained by the phenomenon of cross-relaxation, that is, the radical relaxes via a nearby rapidly relaxing paramagnetic center, that is, [2Fe-2S]-1. It is important to realize that the line broadening and increased rate of relaxation observed in the molybdopterin radical occur under conditions in which the [2Fe-2S]-1 is *oxidized* but in which the increase in line width of [2Fe-2S]-1 and its relaxation behavior have been determined for the reduced cluster (Figure 8). So in order to understand the physical basis for the phenomena observed in the EPR spectra of the molybdopterin radical, it must be shown that the *oxidized* [2Fe-2S]-1 is paramagnetic with a spectral envelope encompassing the $g = 2$ region and that it is rapidly relaxing with a temperature behavior similar to that of the reduced iron−sulfur cluster. As to the latter, since EPR spectra of an oxidized [2Fe-2S] center have never been observed, we will assume that the pathways and/or the temperature dependence of the kinetics to transfer absorbed microwave radiation to the "bath" are similar for the oxidized and reduced iron−sulfur clusters. The ground state of oxidized [2Fe-2S]-1 is $S = 0$, due to antiferromagnetic coupling between the two Fe(III) atoms (*57*). Applying the simple Heisenberg exchange spin Hamiltonian for this system

$$H = J\boldsymbol{S}_1\boldsymbol{S}_2$$

yields $S = 1$ as the first excited state separated at J from the ground state. Typical values for J in [2Fe-2S] proteins range between 300 and 400 cm^{-1} although larger values have also been measured (*58*). This means that in the temperature range of interest to us (65−168 K), the $S = 1$ level is populated for only 0.13−7.7% (taking $J = 300$ cm^{-1}) whereas the higher spin multiplets ($S = 2-5$) are essentially nonpopulated. That the shape of the EPR signal of the whole population of the radical is affected (which itself represents maximally only 15% of the enzyme or [2Fe-2S]-1 concentration), whereas only a small fraction of [2Fe-2S]-1 is in the $S = 1$ state, is possible when the intrinsic relaxation rate of [2Fe-2S]-1 in the $S = 1$ state is much higher than the intrinsic relaxation rate of the molybdopterin radical, a reasonable assumption. In this case, each radical will experience an iron−sulfur center with its magnetic moment resulting from an averaging over the different spin multiplets, a situation similar to that observed for the magnetic interaction between the tyrosyl radical and the diiron-oxo center in ribonucleotide reductase (*39*) or for the interaction of dinuclear (antiferromagnetically coupled) Cu(II) centers with protons as revealed by ^{1}H NMR (*59*, *60*). The average magnetic moment of

[2Fe-2S]-1 and its rate of relaxation increase with increasing temperatures. Thus at relatively low temperatures (<65 K) the population of the $S = 1$ level or the intrinsic rate of relaxation of [2Fe-2S]-1 or both factors together, are too small to induce observable line broadening in the EPR spectrum of the molybdopterin radical.

As noted above, the EPR spectrum of an [2Fe-2S] center in the $S = 1$ state has not been observed, but it is likely to encompass the $g = 2$ region. Both Fe(III) atoms are $^6S_{1/2}$ ions, with g values very close to $g = 2.0023$ (*41*, *57*). Fine structure terms due to the anisotropic part of the exchange interaction, although expected to be small, will undoubtly contribute to the spectrum, but will not be able to shift the main intensity significantly away from the $g = 2$ region. The EPR spectrum of the $S = 1$ excited state of [2Fe-2S]-1 thus overlaps with the EPR spectrum of the molybdopterin radical providing an efficient cross-relaxation pathway.

The observation of dipolar magnetic interaction between reduced [2Fe-2S]-1 and Mo(V) as described before in various molybdoproteins including the aldehyde dehydrogenase from *C. testosteroni* (*23*) is consistent with the relatively short distance between these redox centers found in the crystal structure of the aldehyde oxidoreductase from *D. gigas*. The observation of magnetic interaction between oxidized [2Fe-2S]-1 and the new radical suggests that these centers are quite close and provides additional independent support for the identification of the radical as the molybdopterin radical.

Putative Function of the Molybdenum(VI) Trihydropterin Radical. To establish a role in catalysis of the molybdenum(VI)−trihydropterin radical transient kinetic experiments with any of the three aldehyde dehydrogenases should be performed. So far we have only performed equilibrium trial experiments (data not shown in this paper). Addition of aldehydes did not affect the amount of radical present. However, the redox potential of aldehydes may be too high to affect the amount of radical since they induced only partial reduction of [2Fe-2S]-1 and flavin and no reduction of [2Fe-2S]-2 (*22*, *23*). Addition of dithionite abolished the radical EPR signal. The activity of dithionite-reduced enzyme, which was subsequently reoxidized (no molybdopterin radical), was the same as that of the untreated, as isolated enzyme. This finding indicates either that enzyme molecules with a molybdopterin radical are inactive and cannot be reactivated by this treatment or that the molybdopterin radical is a true intermediate in catalysis. It is not clear in which structural and/or catalytic respect(s) the three bacterial aldehyde dehydrogenases described in this work are different from all other molybdo (tungsto) pterin containing enzymes in which this molybdopterin radical has not been observed so far. Note, however, that the W pterin containing aldehyde oxidoreductase from *P. furiosus* also seems to contain an odd number of electrons in the completely oxidized state (*61*). The odd electron is located on the tungsten atom yielding a W(V) tetrahydropterin. Clearly, this W(V) tetrahydropterin contains two more reducing equivalents than the Mo(VI) trihydropterin. The detection of these two different redox states containing an odd number of electrons may be indicative for a direct role in electron transfer of the pterin moiety, that is, the pterin ring system might act as a one-electron carrier, shuttling between its trihydro and tetrahydro redox states, mediating electron transfer between the molybdenum ion and the nearest iron−sulfur center. The distance in the *D. gigas* aldehyde oxidoreductase between the Mo atom and the nearest Fe atom of the [2Fe-2S] cluster is about 15 Å, the distance between the Mo atom and N5 about 5.5 Å, and from N5 to the Fe atom about 10 Å. Calculation of the rate of electron transfer as a function of the distance as described in ref *62* indicates that the two-step electron-transfer pathway with the molybdo pterin radical as an intermediate is much faster than the single-step electron transfer. However, since also the lowest calculated rate (1000−5000/s) is still much higher than the rate of turnover (100/s), a two-step electron-transfer pathway is not likely to be selected in evolution for its speed, although it may have been so for mechanistic or chemical reasons yet to be uncovered.

ACKNOWLEDGMENT

We thank Drs. P. Gast, A. J. Hoff, and J. S. van den Brink (Department of Biophysics and BIOMAC Research School, Leiden University, Leiden, The Netherlands) for making available their Q-band EPR spectrometer and for their help in these experiments. We also thank Dr. A. Jongejan for his assistence in the use of various modeling and drawing programs on the computer.

REFERENCES

1. Bray, R. C. (1988) *Q. Rev. Biophys. 21*, 299−329.
2. Hille, R. (1996) *Chem. Rev. 96*, 2757−2816.
3. Johnson, J. L., and Rajagopalan, K. V. (1982) *Proc. Natl. Acad. Sci. U.S.A. 79*, 6856−6860.
4. Rajagopalan, K. V. (1991) *Adv. Enzymol. Relat. Areas. Mol. Biol. 64*, 215−290.
5. Krüger, B., and Meyer, O. (1986) *Eur. J. Biochem. 157*, 121−128.
6. Krüger, B., and Meyer, O. (1987) *Biochim. Biophys. Acta 912*, 357−364.
7. Rajagopalan, K. V., and Johnson, J. L. (1992) *J. Biol. Chem. 267*, 10199−10202.
8. Chan, M. K., Mukund, S., Kletzin, A., Adams, M. W. W., and Rees, D. C. (1995) *Science 267*, 1463−1469.
9. Romão, M. J., Archer, M., Moura, I., Moura, J. J. G., LeGall, J., Engh, R., Schneider, M., Hof, P., and Huber, R. (1995) *Science 270*, 1170−1176.
10. Schindelin, H., Kister, C., Hilton, J., Rajagopalan, K. V., and Rees, D. C. (1996) *Science 272*, 1615−1621.
11. Boyington, J. C., Gladyshev, V. N., Khangulov, S. V., Stadtman, T. C., and Sun, P. D. (1997) *Science 275*, 1305−1308.
12. Hilton, J. C., and Rajagopalan, K. V. (1996) *Arch. Biochem. Biophys. 325*, 139−143.
13. Soyka, R., Pfleiderer, W., and Prewo, R. (1990) *Helv. Chim. Acta 73*, 808−826.
14. Fischer, B., Schmalle, H. W., Baumgartner, M. R., and Viscontini, M. (1997) *Helv. Chim. Acta 80*, 103−110.
15. Solomon, P. S., Lane, I., Hanson, G. R., and McEwan, A. G. (1997) *Eur. J. Biochem. 246*, 200−203.
16. Kisker, C., Schindelin, H., and Rees, D. C. (1997) *Annu. Rev. Biochem. 66*, 233−267.
17. Moura, J. J. G., Xavier, A. V., Burschi, M., LeGall, J., Hall, D. O., and Cammack, R. (1976) *Biochem. Biophys. Res. Commun. 72*, 782−789.
18. Barata, B. A. S., Le Gall, J., and Moura, J. J. G. (1993) *Biochemistry 32*, 11559−11568.
19. Huber, R., Hof, P., Duarte, R., Moura, J. J. G., Moura, I., Liu, M.-Y., LeGall, J., Hille, R., Archer, M., and Romão, M. J. (1996) *Proc. Natl. Acad. Sci. U.S.A. 93*, 8846−8851.
20. Poels, P. A., Groen, B. W., and Duine, J. A. (1987) *Eur. J. Biochem. 166*, 575−579.

21. Van Ophem, P. W., Bystrykh, L. V., and Duine, J. A. (1992) *Eur. J. Biochem. 206*, 519−525.
22. Kim, S. W., Luykx, D. M. A. M., de Vries, S., and Duine, J. A. (1996) *Arch. Biochem. Biophys. 325*, 1−7.
23. Luykx, D. M. A. M., Kim, S. W., de Vries, S., and Duine, J. A. (1998) *Biochem. J.*, submitted for publication.
24. Doyle, W. A., Chovnick, A., Whittle, J. R. S., and Bray, R. C. (1996) *Eur. J. Biochem. 239*, 782−795.
25. Gardlik, S., and Rajagopalan, K. V. (1991) *J. Biol. Chem. 266*, 4889−4895.
26. Archer, M. C., Vonderschmitt, D. J., and Scrimgeour, K. G. (1972) *Can. J. Biochem. 50*, 1174−1182.
27. Fischer, D. B., Kirkwood, R., and Kaufman, J. (1972) *J. Biol. Chem. 247*, 5161−5167.
28. Pitterle, D. M., and Rajagopalan, K. V. (1993) *J. Biol. Chem. 268*, 13499−13505.
29. Wuebbens, M. M., and Rajagopalan, K. V. (1993) *J. Biol. Chem. 268*, 13493−13498.
30. Pitterle, D. M., Johnson, J. L., and Rajagopalan, K. V. (1993) *J. Biol. Chem. 268*, 13506−13509.
31. Cardenas, J., and Mortenson, L. E. (1974) *Anal. Biochem. 60*, 372−381.
32. Van den Brink, J. S., Gast, P., and Hoff, A. J. (1996) *J. Chem. Phys. 104*, 1805−1812.
33. Pake, G. E., and Estle, T. L. (1973) in *The Physical Principles of Electron Paramagnetic Resonance*, W. A. Benjamin, Inc., Reading, MA.
34. Müller, F., Hemmerich, P., and Ehrenberg, A. (1971) in *Flavins and Flavoproteins* (Kamin, H., Ed.) pp 107−122, University Park Press, Baltimore, MD.
35. Hagen, W. R. (1992) *Adv. Inorg. Chem. 38*, 165−222.
36. Müller, F., Eriksson, L. E. G., and Ehrenberg, A. (1970) *Eur. J. Biochem. 12*, 93−103.
37. Palmer, G., Müller, F., and Massey, V. (1971) in *Flavins and Flavoproteins* (Kamin, H., Ed.) pp 123−140, University Park Press, Baltimore, MD.
38. Edmonson, D. E., Ackrell, B. A. C., and Kearney, E. (1981) *Arch. Biochem. Biophys. 208*, 69−74.
39. Sahlin, M., Petersson, L., Gräslund, A., Ehrenberg, A., Sjöberg, B.-M., and Thelander, L. (1987) *Biochemistry 26*, 5541−5548.
40. Hoganson, C. W., and Babcock, G. T. (1992) *Biochemistry 31*, 11874−11880.
41. Abragam, A., and Bleany, B. (1970) in *Electron Paramagnetic Resonance of Transition Ions*, Clarendon Press, Oxford, U.K.
42. Antholine, W. E., Kastrau, D. H. W., Steffens, G. C. M., Buse, G., Zumft, W., and Kroneck, P. M. H. (1992) *Eur. J. Biochem. 209*, 875−881.
43. Bobst, A. (1967) *Helv. Chim. Acta 50*, 2222−2225.
44. Bobst, A. (1968) *Helv. Chim. Acta 51*, 607−613.
45. Ehrenberg, A., Hemmerich, P., Müller, Okada, T., and Viscontini, M. (1967) *Helv. Chim. Acta 50*, 411−416.
46. Westerling, J., Mager, H. I. X., and Berends, W. (1975) *Tetrahedron 31*, 437−441.
47. Westerling, J., Mager, H. I. X., and Berends, W. (1977) *Tetrahedron 33*, 2587−2592.
48. Westerling, J. (1978) in *The Identification of Flavin and Pteridine Free Radicals by Electron Spin Resonance*, Thesis Delft University of Technology, Dutch Efficiency Bureau, Pijnacker, The Netherlands.
49. Funahashi, Y., Kohzuma, T., Odani, A., and Yamauchi, O. (1994) *Chem. Lett.* 385−388.
50. Palmer, G., and Massey, V. (1969) *J. Biol. Chem. 244*, 2614−2620.
51. Mayhew, S. G. (1971) *Biochim. Biophys. Acta 235*, 276−288.
52. Smith, W. W., Burnett, R. M., Darling, G. D., and Ludwig, M. L. (1977) *J. Mol. Biol. 117*, 195−225.
53. Smith, W. W., Ludwig, M. L., Pattridge, K. A., Tsernoglou, D., and Petsko, G. A. (1978) in *Frontiers of Biological Energetics: From Electrons to Tissues* (Dutton, P. L., Leigh, J. S., and Scarpa, A., Eds.) Vol. 2, pp 957−964, Academic Press, New York.
54. Lowe, D. J., and Bray, R. C. (1978) *Biochem. J. 169*, 471−479.
55. Barber, M. J., and Siegel, L. M. (1982) in *Flavins and Flavoproteins* (Massey, V., and Williams, C. H., Eds.) pp 796−804, Elsevier/North-Holland, New York.
56. Barber, M. J., Salerno, J. C., and Siegel, L. M. (1982) *Biochemistry 21*, 1648−1656.
57. Gibson, J. F., Hall, D. O., Thornley, J. H. M., and Whatley, F. R. (1966) *Proc. Natl. Acad. Sci. U.S.A. 56*, 987−990.
58. Noodleman, L., and Baerends, E. J. (1984) *J. Am. Chem. Soc. 106*, 2316−2327.
59. Zelonka, R. A., and Baird, M. C. (1972) *Inorg. Chem. 11*, 134−137.
60. Murthy, N. N., Karlin, K. D., Bertini, I., and Luchinat, C. (1997) *J. Am. Chem. Soc. 119*, 2156−2162.
61. Arendsen, A. F., de Vocht, M., Bulsink, Y. B. M., and Hagen, W. R. (1996) *J. Biol. Inorg. Chem. 1*, 292−296.
62. Moser, C. C., Page, C. C., Farid, R., and Dutton, P. L. (1995) *J. Bioenerg. Biomembr. 27*, 263−274.

BI972972Y